Plastic flow and dislocation strengthening in a dislocation density based formulation of plasticity

M. Sudmanns[a], P. Gumbsch[a,b], K. Schulz[a]

[a] *Institute for Applied Materials (IAM-CMS), Karlsruhe Institute of Technology, Kaiserstr. 12, 76131 Karlsruhe, Germany*
[b] *Fraunhofer Institute for Mechanics of Materials (IWM), Wöhlerstr.11, 79108 Freiburg, Germany*

Abstract

Modeling dislocation interaction on a mesoscopic scale is an important task for the description of flow stress and strain hardening in a continuum model. In dislocation based continuum theories, different flow stress formulations are commonly used in the literature. They are usually based on the average dislocation spacing related to the square root of dislocation density, but differ in their degree of homogenization of dislocation interactions, namely whether only total dislocation density is considered in a Taylor term or whether an interaction matrix is used. We analyze the impact of both terms in different crystal orientations as well as homogeneously and inhomogeneously distributed initial dislocation densities. In the dislocation based continuum formulation used here, both terms act as a short-range stress additionally to the "mean field" long-range stress field of elastic dislocation interaction. We demonstrate that the simplifying assumption of an average over all possible interaction types is a reasonable reduction of complexity in high symmetry systems with homogeneous density distribution. However, we also demonstrate that under specific boundary conditions and for inhomogenities between slip systems a significantly different density evolution is obtained on slip systems with similar Schmid-factors, when considering different interaction strengths for different types of dislocation interaction. This is in agreement with findings in discrete dislocation dynamics simulations in the literature.

Keywords: Dislocation dynamics, dislocation interaction, continuum theory, flow stress, strain hardening

1. Introduction

In classical, macroscopic continuum models, flow stress and strain hardening are usually provided by phenomenological parameters based on experimental data. Thus, the material behavior is determined by parameters, which are only valid on the macroscopic scale. It is well known, that continuum models based on these macroscopic parameters are not able to account for microscopic effects such as size effects. Flow stress and strain hardening are input parameters to such models and cannot be considered as a predictive outcome. Physically, dislocation interaction processes and obstacle interactions can be made responsible for the macroscopically measurable flow stress and strain hardening.

Various formulations exist which enhance classical macroscopic approaches by microscopic considerations. One example are strain gradient plasticity models, e.g. [1, 2, 3, 4, 5], which apply

a critical yield stress and a flow rule according to a work hardening rate. Although the formulations show good results in a certain regime, the models are based on a rather phenomenological top-down approach. Thus the interpretation of these models is often limited to the specific system they intend to represent.

In contrast to that, other approaches to continuum formulations are derived bottom-up by homogenizing discrete dislocation lines and their interactions [6, 7, 8, 9]. These models formulate flow stress and strain hardening by physical considerations like the classical Taylor interaction stress [10], which relates a local interaction stress to the mean dislocation distance given as the inverse of the square root of the dislocation density ρ:

$$\tau_{\mathrm{fl},s} = \alpha \mu b \sqrt{\rho} \tag{1}$$

Here, μ is the shear modulus, b is the Burgers vector, and α is a constant factor of 0.35 ± 0.15 [11]. An extended Taylor relation has been developed by Franciosi et al. [12]

$$\tau_{\mathrm{fl},s}^{\mathrm{mat}} = \mu b \sqrt{\sum_j a_{sj} \rho_j} \tag{2}$$

accounting for an individual interaction stress on a slip system s based on the interaction strengths between different slip systems j by pairing coefficients a_{sj} and therefore distinguishing between different slip systems, that lead to different dislocation reactions. In contrast to the factor α in the Taylor term, which is dependent on the mode of deformation, see [13], the coefficients a_{sj} in the enhanced term have been determined as an interaction matrix by discrete dislocation dynamics (DDD) simulations [14, 15, 16].

Even though the classical Taylor interaction stress is still a commonly used formulation due to its simplicity using the total dislocation density and combining all possible interactions between slip systems into one coefficient, it has already been shown in 2d single slip, that such a formulation can oversimplify the local processes in a microstructure [17]. The formulation by Franciosi et al. has been applied and further extended e.g. by [18], who replace the self-hardening coefficients with more physical considerations. A mean free path model incorporating dislocation storage and recovery, as well as the influence of line-tension effects on the interaction constants has been presented in [19, 20]. Further investigation of the flow stress and interaction of slip systems in continuum theories has been done by considering obstacle dislocations [21] and dipoles [22].

Although models incorporating the "Franciosi term" in crystal plasticity frameworks, as e.g. [18, 19, 23], have shown accurate results compared to experiments, both, the Taylor term and the Franciosi term, are still commonly used in their basic form in parallel in the literature. A thorough comparison of both formulations is still missing. However, in order to state the reduction of complexity in a continuum model as central objective, it is a necessity to know in which configurations a simplification is adequate without losing physicality.

Comparing the Taylor term and the Franciosi term, a difference in the microstructural behavior is expected if the system is dominated by a specific type of interaction. It has been shown with DDD-simulations, that the collinear reaction leads to a very strong interaction of the respective slip systems and essentially prevents the activation of two slip systems sharing the same Burgers vector [24, 25]. Since the key parameter determining the interaction stress in the considered formulations is the dislocation density, a difference in interaction stress can occur, if the density is inhomogeneously distributed between the different slip systems.

In this paper, we compare both interaction stress formulations in their basic form. Incorporated in a dislocation density based continuum formulation, we use a set of simple example systems to analyze the dislocation density evolution and the impact of the interaction stress terms with respect to different initial density distributions and systems showing homogeneous as well as heterogeneous density evolutions due to their Schmid factors or microstructural constraints. Starting with most simple configurations leading to an inhomogeneous density distribution, we focus on the effect of collinear reactions in a system setup with just two active slip systems, as in [24]. Then, we extend the analysis to a full fcc single crystal with 12 slip systems. We show, that the classical Taylor interaction stress produces reasonable results when assuming a homogeneous density distribution under ideal loading conditions. Averaging all occurring interactions into a single factor can be adequate if the system behavior is not dominated by a specific interaction or stabilized in high symmetry configurations. However, using the the Franciosi relation, even small variations of the resolved shear stress or initial density lead to a distinctive density evolution on slip systems originating from the collinear interaction coefficient. Such a behavior is in agreement with DDD-simulations [24] and has been proposed as a possible explanation for the strong orientation dependency of certain load orientations [20, 24]. For a continuum theory, trying to mimic such a configuration using the classical Taylor relation, leads to an oversimplification of the complex interactions involved. In contrast, the stronger influence of specific interaction mechanisms in the Franciosi relation allow for a deformation behavior, which can be significantly different to the Schmid law.

2. Method

2.1. Dislocation based continuum model

We consider a dislocation based continuum formulation of crystal plasticity based on the classical decomposition of the distortion tensor into an elastic and a plastic part

$$\mathrm{D}\mathbf{u} = \boldsymbol{\beta}^{\mathrm{pl}} + \boldsymbol{\beta}^{\mathrm{el}}. \tag{3}$$

The plastic slip γ_s is the result of dislocation motion on N slip systems defined by the index s, the orthonormal basis $\{\mathbf{d}_s, \mathbf{l}_s, \mathbf{m}_s\}$ and the Burger's vector $\mathbf{b}_s = b_s\mathbf{d}_s$. Therefore, the plastic distortion $\boldsymbol{\beta}^{\mathrm{pl}}$ consists of the sum of the plastic slip over all slip systems

$$\boldsymbol{\beta}^{\mathrm{pl}} = \sum_{s=1}^{N} \gamma_s \mathbf{d}_s \otimes \mathbf{m}_s \, . \tag{4}$$

The evolution of the plastic slip is given by the Orowan equation

$$\partial_t \gamma_s = \partial_t v_s b_s \rho_s \tag{5}$$

where ρ_s is the dislocation density and v_s the velocity on the individual slip system. Regarding the density evolution, we use the Continuum Dislocation Dynamics (CDD) equations introduced by [6]

$$\begin{aligned}
&\partial_t \rho_s = -\nabla \cdot (v_s \boldsymbol{\kappa}_s^{\perp}) + v_s q_s \qquad \text{with} \qquad \boldsymbol{\kappa}_s^{\perp} = \boldsymbol{\kappa}_s \times \mathbf{m}_s \\
&\partial_t \boldsymbol{\kappa}_s = \nabla \times (\rho_s v_s \mathbf{m}_s) \\
&\partial_t q_s = -\nabla \cdot \Big(\frac{q_s}{\rho_s} \boldsymbol{\kappa}_s^{\perp} v_s + \frac{1}{2|\boldsymbol{\kappa}_s|^2} \Big((\rho_s + |\boldsymbol{\kappa}_s|) \boldsymbol{\kappa}_s \otimes \boldsymbol{\kappa}_s - (\rho_s - |\boldsymbol{\kappa}_s|) \boldsymbol{\kappa}_s^{\perp} \otimes \boldsymbol{\kappa}_s^{\perp} \Big) \nabla v_s \Big),
\end{aligned} \tag{6}$$

where $\boldsymbol{\kappa}_s$ denotes the vector of the geometrically necessary dislocations (GND-density) and q_s the curvature density. We assume a linear dependency on the the resolved shear stress on each slip system τ_s, thus the equations can be closed by the velocity law

$$v_s = \frac{b_s}{B}\tau_s \qquad \text{with} \qquad \tau_s = \tau_{\text{ext},s} + \tau_{\text{int},s} \tag{7}$$

where B denotes a friction stress of 5×10^{-5} Pa s. $\tau_{\text{ext},s}$ includes stresses induced by external loading resolved on the slip system, whereas $\tau_{\text{int},s}$ accounts for internal stresses induced by dislocations. Regarding $\tau_{\text{int},s}$, we distinguish between long- and short-range stresses in the continuum model. In order to represent long-range stress fields, we consider a mean field approach as given in [26] resulting in the "mean field stress" $\tau_{\text{mf},s}$. Since the mean field stress is proportional to $\int \kappa$, it accounts for the contribution of the slip on a specific slip system to the long-range stress field on all slip systems. However, the mean field stress disappears in configurations of statistically stored dislocations and neglects interactions of dislocation densities inside an averaging volume. Thus, it delivers no information about the strength of the physical interaction and reactions between different slip systems.

To solve this problem, additional stress formulations are used to describe the interaction between slip systems within one averaging volume. We consider the "Taylor term" according to Eq. (1), which relates the interaction stress to the square root of the total density averaged over all slip systems within one averaging element. Thus, the interaction stress is the same on all slip systems and all possible interaction types are concentrated into the parameter α. In this study, we choose $\alpha = 0.35$, unless otherwise stated. In addition, the "Franciosi term" according to Eq. (2) is incorporated into the formulation, which summarizes the interaction strengths of each individual slip system pairing, a_{sj}, multiplied by the density of the respective slip system ρ_j. Thereby, the different interaction mechanisms are considered separately, which in general leads to different interaction stresses on different slip systems. Regarding the interaction strengths a_{sj}, we consider the interaction matrix according to [14]. For the self-interaction and coplanar cases, i.e. $j = s$ and $j = s \pm 1$, we chose the Lomer coefficient given as 0.122 [20].

The Taylor term as well as the Franciosi term act on the velocity of each slip system. Therefore the velocity law can be derived as

$$v_s = \begin{cases} \frac{b_s}{B}(|\tau_s| - \tau_{\text{fl}})\text{sign}\tau_s & \text{if } |\tau_s| > \tau_{\text{fl}} \\ 0 & \text{if } |\tau_s| \leq \tau_{\text{fl}} \end{cases} \tag{8}$$

where τ_{fl} contains the interaction stress term acc. to Eq. (1) or Eq. (2). Here, both terms can be interpreted as a "friction stress" to reduce density motion, which influences directly the evolution of plastic slip (Eq. (5)) according to the individual formulation of the interaction stress. Therefore, in contrast to the idea of an immobile forest density, the total dislocation density is mobile, but moves with a lower velocity.

In addition, a phenomenological formulation accounting for the increase in line length due to dislocation multiplication described in e.g. [27, 28] is taken into account, which describes the increase of dislocation density per slipped area proportional to a storage rate by a mean free path Γ according to [29] as

$$\frac{d\rho}{d\gamma} = \frac{1}{b\Gamma}. \tag{9}$$

Here, we consider the density production and neglect the dynamic recovery, since the latter becomes relevant only at high strains [28]. Following [27, 28], we assume the mean free path

Γ to be proportional to the mean dislocation spacing on the individual slip system $1/\sqrt{\rho_s}$. The production rate can then be derived as

$$\partial_t \rho_s = c v_s \rho_s^{1.5} \tag{10}$$

with $c = 0.05$ similar to [18, 30]. The evolution equation of the density, Eq. (6), then changes to

$$\partial_t \rho_s = -\nabla \cdot (v_s \boldsymbol{\kappa}_s^{\perp}) + v_s q_s + 0.05 v_s \rho_s^{1.5}. \tag{11}$$

It is noted, that this very simple formulation is only intended to serve as an additional production term to allow for increasing dislocation densities. The formulation is not intended or capable of mechanistically modeling real multiplication mechanisms like cross-slip and glissile reactions. Therefore, we assume that the density production takes place on each slip system irrespective of density on other slip systems. Furthermore we ignore the increase of the curvature density due do the generation of new dislocation loops. This neglects the effect, that cross-slip and glissile reactions lead to a deposition of dislocations on other slip systems, which would require the modeling of dislocation transport between slip systems.

Regarding the numerical formulation, we use the elasto-plastic framework described in [31] incorporated in the finite element code M++, which is based on a parallel multigrid method [32]. We consider the fully three dimensional setup of the CDD evolution equations coupled with the elastic problem as a two-scale approach. For the numerical solution of the CDD evolution equations (Eq. 6), we combine the evolution equations of the dislocation densities to solve them by the system of equations

$$\partial_t \begin{pmatrix} \rho_s \\ \boldsymbol{\kappa}_s \end{pmatrix} + \nabla \cdot \boldsymbol{F}_s \begin{pmatrix} \rho_s \\ \boldsymbol{\kappa}_s \end{pmatrix} = \boldsymbol{G}_s \tag{12}$$

with the flux $\boldsymbol{F}_s$ and the source $\boldsymbol{G}_s$ given as

$$\boldsymbol{F}_s \begin{pmatrix} \rho_s \\ \boldsymbol{\kappa}_s \end{pmatrix} = v_s \begin{pmatrix} \mathbf{l}_s \cdot \boldsymbol{\kappa}_s \mathbf{d}_s - \mathbf{d}_s \cdot \boldsymbol{\kappa}_s \mathbf{l}_s \\ (\mathbf{d}_s \otimes \mathbf{l}_s - \mathbf{l}_s \otimes \mathbf{d}_s)\rho_s \end{pmatrix} \text{ and } \boldsymbol{G}_s = \begin{pmatrix} v_s q_s \\ 0 \end{pmatrix}. \tag{13}$$

Thereby, we distinguish between the dislocation densities and the evolution equation of the curvature density q_s. Both parts are treated as separate transport problems, where the right hand side in Eq. (12) is a production term depending on the curvature density q_s, which itself is considered a conserved quantity for the solution of the dislocation density evolution equations. Therefore the curvature density q_s is the variable, which couples both parts of the transport problem. The equations are solved separately for each slip system. For the integration of both parts of the transport problems, we use a discontinuous Galerkin scheme with an upwind flux formulation using an implicit midpoint rule. Regarding the discretization, the stress computation by the finite element method, as well as the internal variables of the microstructure are solved on the same mesh. However we use linear shape functions for the finite element method and quadratic shape functions for the CDD evolution equations.

2.2. Considered systems

2.2.1. Fcc crystal with 12 slip systems in [001] high symmetry orientation

As a reference case, we analyze an fcc single crystal with 12 slip systems in [001] high symmetry crystal orientation. We use a cubic simulation cell with edge length of $50 \times 50 \times 50\ \mu$m and open boundary conditions for the dislocation flux. To avoid boundary effects, we restrict the

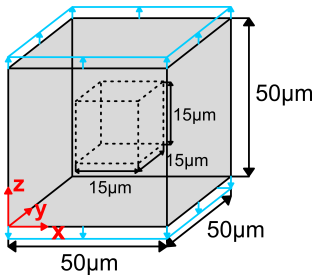

Figure 1: Geometry of the setup with 12 slip systems. The inner cube visualizes the area used for determination of the internal variables.

evaluation of the internal variables to an inner cube with edge length of 15×15×15 μm , see fig. 1. We discretize the system by 46 tetragonal elements per direction on average. Regarding the initial dislocation microstructure, we assume a total density of $\rho_{\text{tot}} = 1.75 \times 10^{13}\ m^{-2}$, which consists of homogeneously distributed dislocation loops with an initial radius of $r_0 = 0.8\mu$m. The density is equally distributed over all slip systems. Additionally, we consider the phenomenological dislocation multiplication according to Eq (11). The material parameters are taken to mimic aluminum with an elastic modulus $E_{Al} = 70$ GPa, a Poisson's ratio $\nu_{Al} = 0.3$ and a Burger's vector of $b_s = 0.256$ nm.

As a first example, we consider a benchmark test by studying the initial yield point compared to DDD-results [11] and experimental data [33, 34]. According to ref. [11], we consider three simulations with the initial densities $\rho_{\text{tot}} = 1.3 \times 10^{11}\ m^{-2}$, $\rho_{\text{tot}} = 1.3 \times 10^{12}\ m^{-2}$, and $\rho_{\text{tot}} = 1.3 \times 10^{13}\ m^{-2}$. Thus, the resulting forest densities are approximately $\rho_{\text{f}} \approx 10^{11}\ m^{-2}$, $\rho_{\text{f}} \approx 10^{12}\ m^{-2}$ and $\rho_{\text{f}} \approx 10^{13}\ m^{-2}$ [11]. As shown in fig. 1, we subject the system to a tensile strain in z-direction using a constant strain rate of $\dot{\epsilon} = 10\ s^{-1}$, which is reasonably close to the value given in [11].

In a second step, we analyze the density evolution on the slip systems. Therefore we subject the system to a constant strain rate of $\dot{\epsilon} = 1000\ s^{-1}$ up to a maximum strain of 0.6%, where we use a rather high strain rate in order to save computation time. In the [001] crystal orientation, four slip systems are inactive due to a vanishing resolved shear stress. The eight active slip systems have the same Schmid-factor and represent pairings of slip and cross-slip systems. Thereby, we investigate the effect of both interaction stress formulations in equal stress and density conditions on all active slip systems.

2.2.2. *Reduced system of two slip systems*

In order to study the influence of the considered stress terms $\tau_{\text{mf},s}$, $\tau_{\text{fl},s}$ and $\tau_{\text{fl},s}^{\text{mat}}$ on the interaction behavior in heterogeneous systems, we restrict our setup to two slip systems, see fig. 2 (left). To allow for a good resolution of the behavior near and within the lamellae, we choose a significantly smaller system size, than in section 2.2.1 using resolution of 92 tetragonal elements per direction on average. We analyze a Lomer and a collinear setup with slip systems $(111)\langle\bar{1}01\rangle$, $(\bar{1}\bar{1}1)\langle 011\rangle$ for the Lomer configuration and $(111)\langle 0\bar{1}1\rangle$, $(\bar{1}11)\langle 0\bar{1}1\rangle$ for the collinear configuration. We consider two intersecting slip lamellae, shown in fig. 2 (left), by restricting the density distribution to a thickness of 2 μm normal to the slip planes. We analyze two density distributions $\rho_1 = \rho_2$ and $4\rho_1 = \rho_2$ with $\rho_1 = 1 \times 10^{12}\ m^{-2}$, where ρ_1 and ρ_2 are the total densities on the primary and the secondary slip system respectively. The densities are introduced as homogeneously distributed dislocation loops with an initial loop radius of $r_0 = 2\mu$m. This radius is significantly

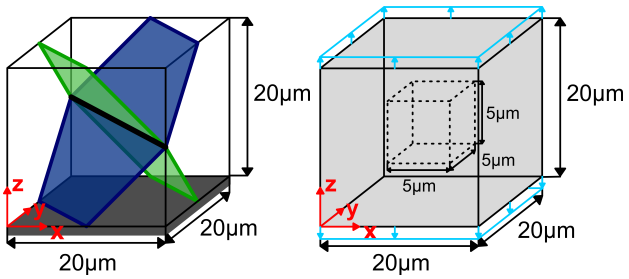

Figure 2: Geometry of the system with two slip lamellae, here schematically visualized for the Lomer configuration (left) and geometry of the system initialized with homogeneous density distribution on two slip systems (right). The inner cube visualizes the area used for determination of the internal variables.

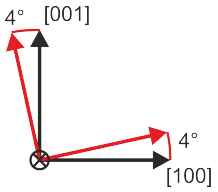

Figure 3: Visualization of crystal orientation rotated by 4° around the [010] crystal axis.

larger than in the high symmetry system described in section 2.2.1 to avoid a relaxation of the system due to high local density increase without significant dislocation transport. In the area, where the lamellae intersect, it holds $\rho_{tot} = \rho_1 + \rho_2$ and outside of the intersection area $\rho_{tot} = \rho_1$ and $\rho_{tot} = \rho_2$ respectively. The system is fixed at the z-faces and both slip systems are subjected to a constant homogeneous stress field of $\tau_{\text{ext}} = 10$ MPa.

In a further analysis, we distribute the density homogeneously over the complete cubic system and subject the system to constant strain rates of $\dot{\epsilon} = 1000\ s^{-1}$ and $\dot{\epsilon} = 200\ s^{-1}$ in the z-direction, as shown in fig. 2 (right). Thereby we compare the influence of the strain rate on the resulting system behavior. For the subsequent analysis, we then use a constant strain rate of $\dot{\epsilon} = 1000\ s^{-1}$ to reduce computational effort. To minimize boundary effects, we restrict our evaluation of the internal variables to an inner cube with edge length of $5 \times 5 \times 5\ \mu$m. Using an equal density distribution of $\rho_1 = \rho_2$ in the collinear slip system configuration, we then rotate the crystal orientation by 4° around the [010]-axis in mathematically positive direction, as shown in fig. 3. This leads to different Schmid-factors on both slip systems, which allows the investigation of both formulations regarding their behavior in a collinear system. The collinear interaction is represented in the interaction matrix [14] with the highest value of all interaction types. The strength and the impact of this interaction was previously confirmed by DDD-simulations [24, 25]. In this part we only investigate the very beginning of the density evolution, thus we only consider density increase due to expansion of existing dislocation loops, described by Eq. (6).

2.2.3. Inhomogeneous density and non high symmetry orientations in a 12 slip system setup

As a final example, we consider the setup with 12 slip systems again. One specific feature of the [001] loading axis is that both slip and cross-slip systems have the maximum Schmid-factor. Thus, this specific configuration allows for an investigation of the effect of the high collinear factor in the interaction matrix on the system behavior. Therefore, we now compare the evolving

density on the slip systems using a crystal orientation rotated by 4° around the [010]-axis, as shown in fig. 3. As a result, the different Schmid-factors vary between 0.3779 and 0.4347 for the eight active slip systems. The Schmid-factors on the other four slip systems are nonzero but comparably low. The initial density configuration is the same as for the high symmetry system.

In a further analysis, we use the density distribution resulting from the rotated crystal orientation as an initial condition in a [001] high symmetry orientation again. In this case, the initial total density is $\rho_{\text{tot}} = 2.2 \times 10^{13}\ m^{-2}$ with a strong heterogeneity between slip systems. The boundary and loading conditions are given as before. For both, the inclined and the high symmetry orientation, we compare the impact of a prevented and an allowed lateral contraction of the Dirichlet boundaries. Allowing lateral contraction also allows for a shift of the crystal out of the uniaxial deformation.

3. Results

In this section we first validate the initial yield point by comparing a high symmetry configuration to DDD-simulations and analyze the evolving density distribution in a system with equal initial density distribution. Then, we investigate the behavior of two representative slip systems in a Lomer and a collinear configuration. Finally, we analyze the impact of the interaction stress formulations on the density distribution in a system with a heterogeneous resolved shear stress as well as heterogeneous initial density configurations. An overview of the investigated configurations is given in Table 1.

configuration	figures
Full system, high symmetry	fig. 4, 5
Reduced system, slip lamellae	fig. 6, 7
Reduced system, homogenized density	fig. 8, 9, 10
Full system, low symmetry and inhomogeneous density	fig. 11, 12

Table 1: Tabular overview of investigated configurations.

3.1. Flow stress and density evolution in a high symmetry setup with 12 slip systems

By considering the [001] setup with 12 slip systems as described in section 2.2.1, we compare the initial yield point to DDD-data and experimental results from [11, 33, 34]. In a continuum, the yield point is taken as the stress, at which dislocation motion starts. Fig. 4 shows that the yield point for the investigated densities coincides with DDD and experimental results. This is expected since the constant hardening factors in both interaction stress formulations reproduce the analytical Taylor function. If the Taylor term is assumed, the chosen average factor of $\alpha = 0.35$ acts on the forest density ρ_f as well as on the densities of the same and coplanar slip systems in a self-hardening way. Remarkably, the difference between both formulations regarding the initial yield point turns out to be negligibly small in this case.

In a second step, we analyze the dislocation density evolution on the individual slip systems using a [001] high symmetry crystal orientation. By choosing an initial density of $\rho_{\text{tot}} = 1.75 \times 10^{13}\ m^{-2}$ equally distributed over all slip systems, we get a resulting density distribution for both interaction stress formulations as shown in fig. 5. Here, the dislocation density is given as an average density per slip system. There is no density evolution on the four slip systems

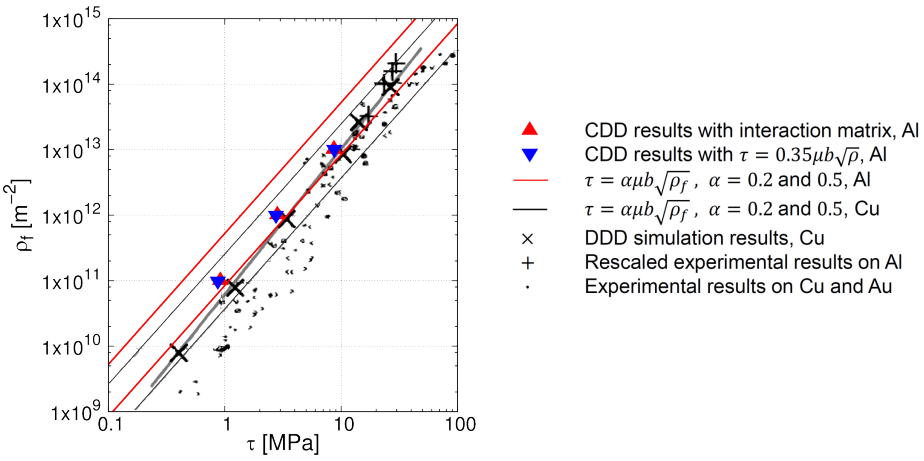

Figure 4: Comparison of first yield point with DDD and experimental data from [11][33][34] using the high symmetry setup with 12 slip systems described in section 2.2.1. The thin red and black lines show analytical results for aluminum and copper. For the DDD simulations and some experiments copper was used as model material, in the continuum we assumed aluminum.

with zero Schmid-factor. The density evolution concentrates on the eight active slip systems and is nearly identical for both formulations at 0.3% strain. At 0.6% strain, there is a somewhat larger difference between both formulations. The differences between slip systems seem to be vanishingly small for the Taylor term and more significant for the interaction matrix.

3.2. Reduced system of two slip systems

To closer investigate the interplay of the different stress terms in different slip system and density configurations, we consider a simple lamellae configuration described in section 2.2.2. This example is artificial and not intended to reproduce a real material, but it provides a simple way to investigate both interaction stress formulations in heterogeneous density distributions. A systematic comparison is shown in fig. 6 and 7. The axes represent a local coordinate system on the primary slip system with the x-axis pointing in the direction of the intersection line. Here, only the density on the primary slip system ρ_1 is shown.

In a first analysis, shown in fig. 6, we only consider the mean field stress $\tau_{\mathrm{mf},s}$ and an equal distribution of the densities between both slip systems with $\rho_1 = \rho_2 = 1\times10^{12}\ m^{-2}$. A clear interaction between both slip systems is observed even without considering any additional interaction stress term. The density accumulates at $Y \approx \pm1\mu$m, where both lamellae intersect. However, the density for $-0.5\mu\mathrm{m} \leq Y \leq 0.5\mu\mathrm{m}$ is the same as outside the intersection area $|Y| > 2\mu$m (fig. 6).

Adding the Taylor term $\tau_{\mathrm{fl},s}$, a more pronounced density accumulation on both sides of the intersecting lamella is observed (fig. 7 (top)). Qualitatively, however, the density evolution is similar to the case above (with mean field stress only, fig. 6) except for an overall reduction of the density evolution, cf. fig. 6 and 7 (a,b). For $4\rho_1 = \rho_2$, more density is concentrated within the intersection due to the more pronounced interaction between the slip systems (fig. 7 (c)).

Investigating the effect of the self-hardening coefficient in the extended formulation with interaction matrix $\tau^{\mathrm{mat}}_{\mathrm{fl},s}$, it is found that self-hardening reduces the overall density on the slip system for equal density distribution between both slip systems as shown in fig. 7 (d,e). In case of $4\rho_1 = \rho_2$ a qualitative difference between the results with and without self-hardening is not

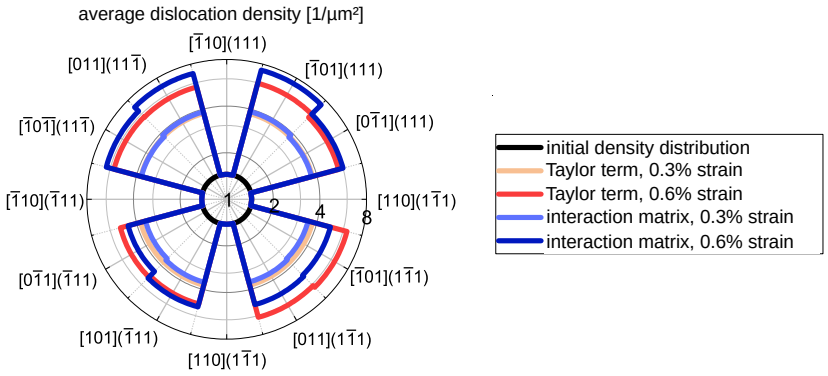

Figure 5: Radial logarithmic plot showing the density distribution on the slip systems for two intermediate strains using a [001] high symmetry crystal orientation with an initial density equally distributed on the slip systems as described in section 2.2.1.

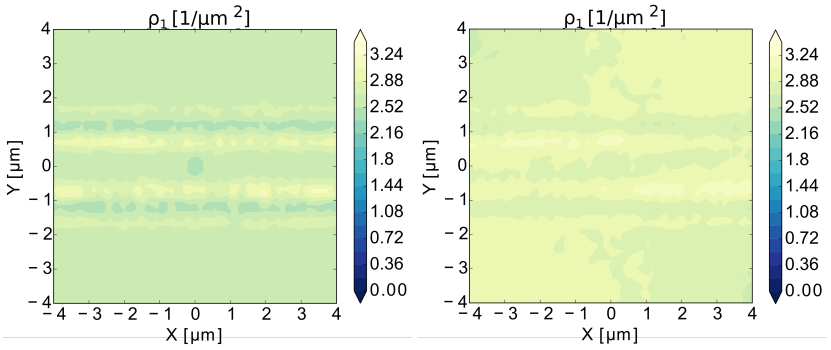

(a) Lomer configuration (b) collinear configuration

Figure 6: Comparison of the density distribution on the first slip system for the reduced system with two slip lamellae described in section 2.2.2. Shown is the $\rho_1 = \rho_2 = 1 \times 10^{12}\ m^{-2}$ density distribution only with the mean field stress $\tau_{\mathrm{mf},s}$ using the Lomer configuration (a) and the collinear configuration (b). The coordinates are local coordinates on the slip plane. Only the ρ_1 density is shown.

visible (fig. 7 (f)). In the Lomer configuration, we get the same resulting density distribution for the interaction matrix and the Taylor term (fig. 7 (a,d)). This is because both acting coefficients in the interaction matrix have the same value as the average coefficient used in the Taylor term. However, for a high deviation of the interaction strengths from the average, i.e. the collinear factor in the present example, less similarities between both formulations are visible, cf. fig. 7 (e,f). This effect further increases in the heterogeneous density distribution.

In a next step, we distribute the density homogeneously over the complete cubic system. First, we consider an equal distribution of the initial density between the slip systems. By subjecting the system to a constant strain rate, we get a stress-strain curve with an elastic part followed by a plastic deformation after an increase of the stress on the slip systems over the respective yield point (fig. 8 (a)). To investigate the influence of the strain rate, we concentrate on the Lomer configuration for both interaction stress terms. Without the self-hardening coefficient in the interaction matrix, we observe a lower yield point compared to the Taylor term, which is even

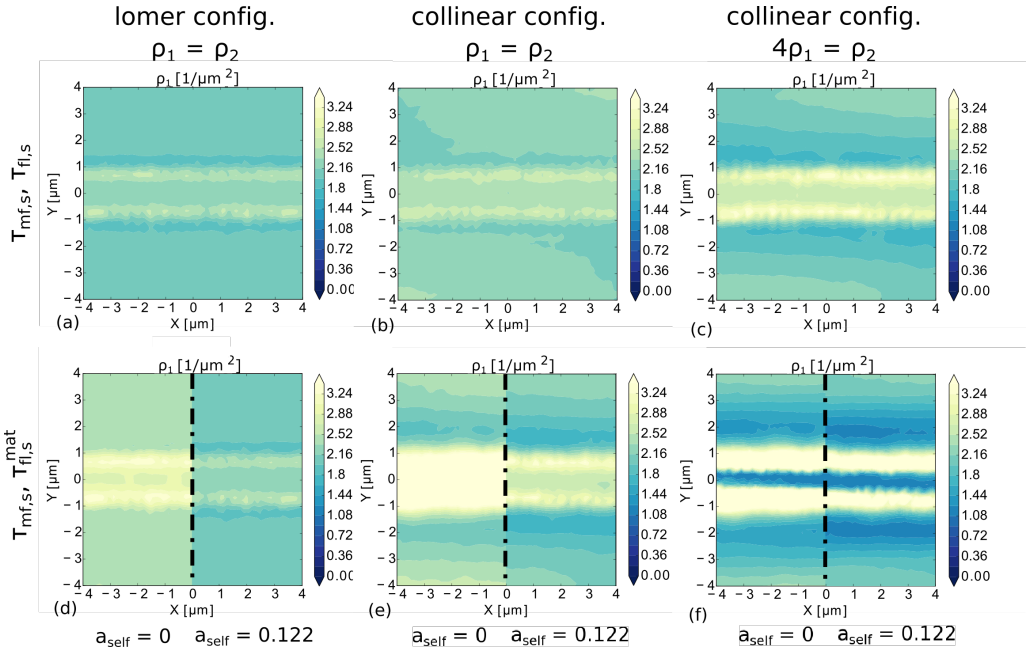

Figure 7: Comparison of the density distribution on the first slip system for the reduced system with two slip lamellae described in section 2.2.2. Shown is the Lomer and collinear configuration with $\rho_1 = \rho_2$ and the collinear configuration with $4\rho_1 = \rho_2$ with $\rho_1 = 1 \times 10^{12}\ m^{-2}$. First row shows the result with mean field stress $\tau_{\mathrm{mf},s}$ and the Taylor term $\tau_{\mathrm{fl},s}$ (a,b,c), second row shows the result with $\tau_{\mathrm{mf},s}$ and the extended formulation with interaction matrix $\tau^{\mathrm{mat}}_{\mathrm{fl},s}$ with $a_{\mathrm{self}} = 0$ (d,e,f) left and with $a_{\mathrm{self}} = 0.122$ (d,e,f) right.

more pronounced for different densities on the slip systems, cf. fig. 8 (b). In all cases, a faster transition from the elastic part to a stable plastic flow is observed for the lower strain rate, thus affecting the yield point. However, the slope of the stress strain curve after the yield point is not affected by the different strain rates for both investigated density configurations and interaction stress terms.

Based on the moderate influence of the strain rate for the considered system setup, in the following a strain rate of $1000 s^{-1}$ is applied in order reduce computation time. We compare the influence of different slip system configurations on the system behavior for both formulations and density distributions. For the interaction matrix, a significantly higher yield point can be observed in the collinear slip system configuration compared to the Lomer configuration, as shown on fig. 9 (a). Using the Lomer configuration with the self-hardening coefficient in the interaction matrix, the stress strain curve is identical to the Taylor formulation. However, the influence of the self-hardening is small in the collinear configuration, which is in agreement with the results of the lamellae system, cf. fig. 7 (f). The Taylor term is obviously not able to capture the different strengths of both interaction types with one average parameter. However, in the present density configuration, the Taylor term can reproduce the behavior of the interaction matrix by fitting different average factors, as shown in fig. 9 (a).

If the initial density on one slip system is increased, a heterogeneity is introduced in the system, as shown in fig. 9 (b). For the Lomer configuration with self-hardening, the stress-strain curves are still identical to the Taylor formulation. This is expected since $\sqrt{a_{\mathrm{Lomer}}} =$

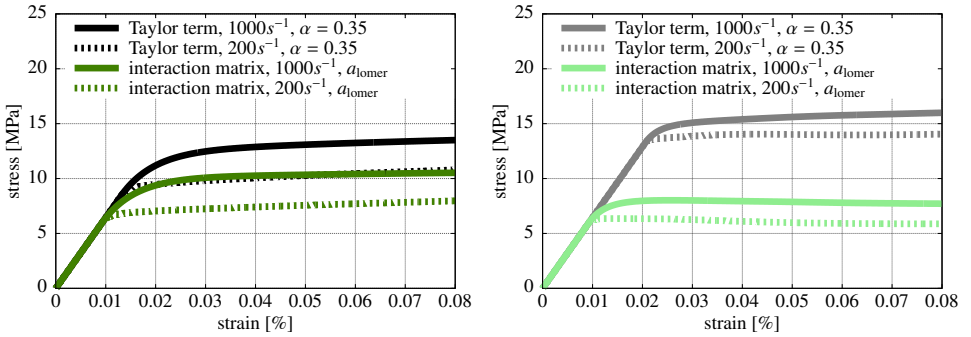

(a) $\rho_1 = 1 \times 10^{12}$ 1/m^2 $= \rho_2$ (b) $\rho_1 = 1 \times 10^{12}$ 1/m^2, $\rho_2 = 4 \times 10^{12}$ 1/m^2 $= 4\rho_1$

Figure 8: Comparison of the stress-strain curves for the homogenized system with two slip systems described in section 2.2.2 for the Lomer configuration using a strain rate of $1000s^{-1}$ and $200s^{-1}$. The system is initialized with a density distribution of $\rho_1 = \rho_2$ (a) and $4\rho_1 = \rho_2$ (b) for both interaction stress terms.

$\sqrt{a_{\text{self}}} \approx 0.349$, which is almost identical to the assumed average coefficient of 0.35. Thus the resulting interaction stresses are also the same. However, in case of the collinear configuration, the Taylor term using the average factor of 0.61 overestimates the interaction stress compared to the interaction matrix, see fig. 9(b). This is because the average factor is acting on both slip systems, thus the self-hardening is weighted with a factor of 0.61.

For an increased Taylor factor, we observe a shift of the average plastic slip evolution to higher strains without qualitatively changing the behavior of both slip systems. This can be seen in fig. 10 (a). In contrast, using the interaction matrix with the high collinear factor, a concentration of the plastic slip on the slip system with higher initial density and an inhibition of the simultaneous activation of both collinear slip systems is observed (fig. 10 (a)).

A similar behavior is observed for a system with equally distributed density, but different Schmid-factors on both slip systems. The resulting evolution of the plastic slip for both formulations is shown in fig. 10 (b) in comparison to the ideal [001] high symmetry orientation. In the high symmetry orientation, the plastic slip evolves nearly identical for both formulations. In the rotated orientation, the plastic slip spreads according to the different Schmid-factors when using the Taylor term. This leads to the activation of both collinear slip systems. In contrast, the collinear factor in the interaction matrix leads to an inhibition of the plastic slip on the slip system with the lower Schmid-factor up to 0.15% strain. For higher strains, the plastic slip saturates since dislocations start leaving the system. Together with the saturation on the dominating slip system, the plastic slip on the second slip system increases.

3.3. Inhomogeneous density and low-symmetry orientation with all 12 slip systems

As a final example, we analyze the dislocation density evolution on the individual slip systems in a near [001] crystal orientation. Here, we use all 12 slip systems as introduced in section 2.2.3. Considering a crystal orientation rotated by 4° around the [010] axis, two of the four pairings of collinear slip system have different Schmid-factors, the other two pairings have the same Schmid-factor. First, we allow a lateral contraction of the Dirichlet boundaries and therefore also a lateral shift of the top and bottom faces. Compared to the high symmetry case shown in fig. 5, the resulting density distribution in the rotated crystal orientation turns out to be heterogeneous for both interactions stress formulations. This is displayed in fig. 11 (a). Using the Taylor term,

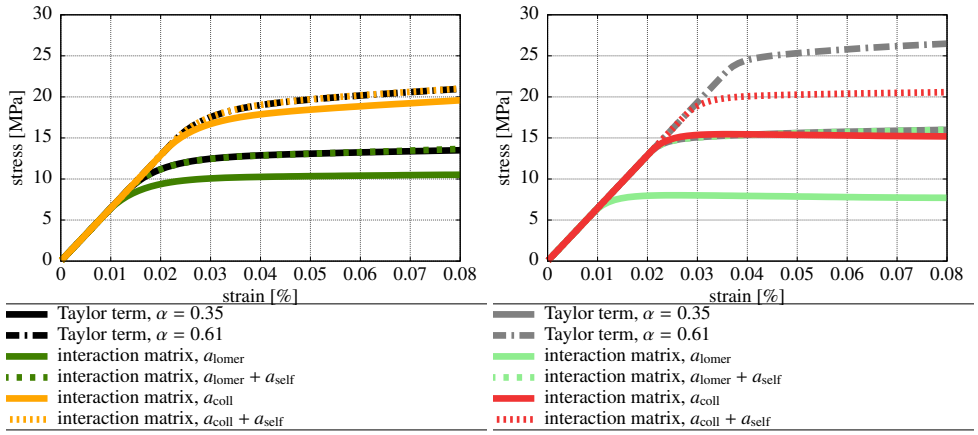

(a) $\rho_1 = 1 \times 10^{12}\ 1/\text{m}^2 = \rho_2$ (b) $\rho_1 = 1 \times 10^{12}\ 1/\text{m}^2, \rho_2 = 4 \times 10^{12}\ 1/\text{m}^2 = 4\rho_1$

Figure 9: Comparison of the stress-strain curves for the homogenized system with two slip systems described in section 2.2.2 for the Lomer and the collinear configuration for $\rho_1 = \rho_2$ (a) and $4\rho_1 = \rho_2$ (b) for both interaction stress terms. The coefficients are $a_{\text{Lomer}} = 0.122$, $a_{\text{koll}} = 0.625$, $a_{\text{self}} = 0.122$.

the density evolves according to the stresses given by the Schmid-factors. Slip systems with the same Schmid-factor show the same behavior independent of their crystal orientation. In contrast, with the interaction matrix, the density evolution between slip systems with the same Schmid-factor can be different. A strong interaction between the slip and cross-slip systems, which is consistent with the results shown in section 3.2 is noticed here. Using the interaction matrix, three slip systems remain deactivated. One slip system shows no further density evolution after 0.3% strain. None of the four slips systems, which show significant dislocation activity at 0.6% strain share a common Burger's vector. This is a strong contrast to the Taylor term, which does not show this behavior.

A similar tendency can be observed, when starting with a heterogeneous initial density distribution in the [001] high symmetry system, as shown in fig. 11 (b). In case of the Taylor term the density increases proportionally to the initial average density. In contrast, by using the interaction matrix, we see a significant interaction between pairings of collinear systems. Although the difference in the density distribution is not as pronounced as in the case of the rotated crystal, the tendency is the same.

The strong effect of the collinear coefficient in the interaction matrix is highly dependent on the freedom of the system to allow lateral displacement. This can be illustrated by an example, which prevents the lateral contraction and the shift of the Dirichlet boundaries in the system and therefore enforce a purely uniaxial tensile deformation. The resulting density distribution on the slip systems are shown in fig. 12 (a,b). Compared to the elastically more flexible deformation above, we observe very little difference between both interaction stress formulations, cf. fig. 11 (a,b) and fig. 12 (a,b). Furthermore, the results for the Taylor term are significantly different from the previous case, cf. fig. 11 (a) and 12 (a). This shows, that the higher stiffness regarding lateral contraction leads to higher stresses on all slip systems. If lateral shift is allowed, the slip systems with the maximum Schmid-factor lead to deformation lateral to the tensile orientation. Thus, the flexible boundary conditions include the potential to relax the applied elastic deformation

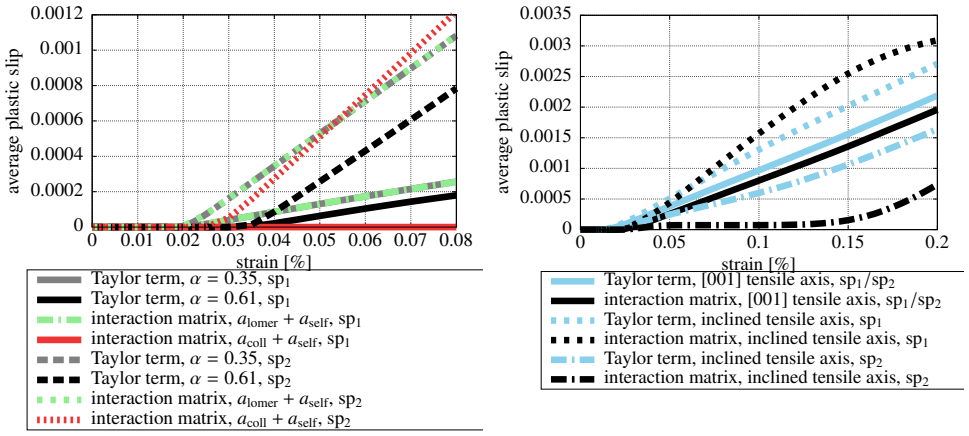

(a) $4\rho_1 = \rho_2$, tensile in high symmetry orientation, cf. fig. 9 (b)

(b) $\rho_1 = \rho_2$, 4° inclined tensile axis

Figure 10: Evolution of the average plastic slip on both slip systems for both interaction stress formulations in the homogenized system with two slip systems using the Lomer and collinear configuration, $4\rho_1 = \rho_2$ (a) and a collinear configuration with a crystal orientation rotated by 4° around the [010]-orientation, see fig. 3, $\rho_1 = \rho_2$ (b).

increases.

4. Discussion

In dislocation based continuum formulations of plasticity, one essential issue is a physically plausible formulation of flow stress and strain hardening behavior. In CDD, interaction between different slip systems due to the intrinsic stress fields of dislocations are considered by the mean field stress. However, the interaction by the mean field stress disappears for statistically stored dislocations and thus it is dependent on the resolution of the microstructure. To solve this problem, additional interaction stress terms are used, which allow for a density-dependent interaction within one averaging element. Applying two commonly used interaction stress formulations - the classical Taylor term and the extended interaction matrix by Franciosi et al. [12] - differences and similarities of both terms in specific configurations are discussed in this paper.

Using a cubic system with open boundaries incorporating all 12 fcc slip systems, both considered interaction stress terms are analyzed regarding the initial yield point. Fig. 4 shows this interaction stress as a function of the forest density for both formulations in comparison with DDD-results from [11] and experimental results from [33] and [34]. Here, we assume the Taylor coefficient α and the hardening coefficients in the interaction matrix a_{sj} constant for different forest densities, which leads to a direct reproduction of the analytical functions. Although the hardening coefficients are largely different for different interaction mechanisms, summing up the contributions of a completely homogeneous initial density distribution does not lead to any difference compared to the classical Taylor formulation. Regarding the density evolution on the slip systems, it is shown in fig. 5, that an almost equal increase of the density on all non-zero Schmid-factor slip systems is achieved for the reference case of an equal distribution of the initial density in the [001] high symmetry orientation. This observation holds for both interaction stress

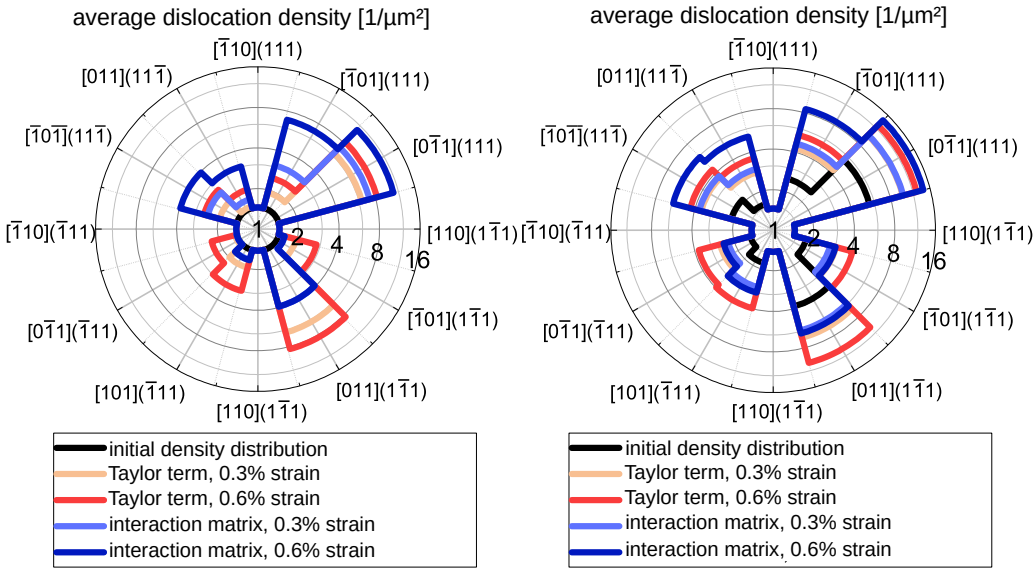

(a) 4° rotated crystal orientation, homogeneous initial density distribution

(b) [001] high symmetry orientation, heterogeneous initial density distribution

Figure 11: Radial logarithmic plots showing the density distribution on all 12 slip systems for the setup described in section 2.2.3 for two intermediate strains using a rotated crystal orientation by 4° around the [010]-axis with an equal initial density distribution (a) and a [001] high symmetry crystal orientation with an inhomogeneous initial density distribution (b). Here, the lateral contraction and shift of the Dirichlet boundaries is allowed.

terms, thus it can be concluded that the classical Taylor term is a very reasonable simplification for such systems.

However, regarding the self-reinforcing nature of the density-dependent interaction stress, differences between both formulations are expected in heterogeneous configurations regarding density or stress distribution on the slip systems. For simplicity, the considered system is reduced to two intersecting slip lamellae representing two slip systems in Lomer and collinear configuration. Since the mean field stress affects all involved slip systems, there are pile-ups observed at the intersection of the lamellae even without an additional interaction stress, shown in fig. 6. Thus it can be expected, that for an increasing spatial resolution, there will also be a more precise resolution of the interaction in the vicinity of the intersection. However, a continuum formulation aims to consider resolutions as coarse as possible, thus the interaction stress term inheres the character of a short-range interaction stress. The interaction due to the mean field stress just represents the accumulation of GND-density and does not account for specific reaction types. Thus, in the CDD formulation, the density within the intersection is not affected by the density of the second slip system other than stresses originating from GND pile-ups, and thus dependent on the resolution.

Furthermore, the Taylor interaction stress (chosen with an average factor of $\alpha = 0.35$) not only affects the interaction of both slip systems, but also the density on the same slip system in a self-hardening way (fig. 7). Thus, the density evolution is artificially reduced in areas without occurring interaction with other slip systems. These results indicate that the self-hardening nature of the classical Taylor interaction stress inhibits the overall dislocation mobility with very little

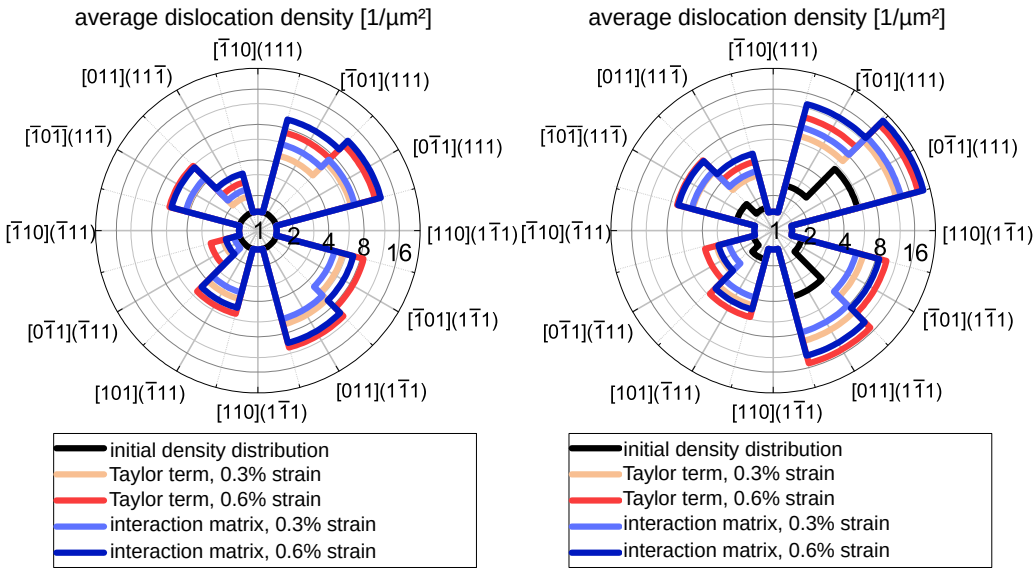

(a) 4° rotated crystal orientation, homogeneous initial density distribution

(b) [001] high symmetry orientation, heterogeneous initial density distribution

Figure 12: Same as fig. 11 with prevented lateral contraction and shift of the dirichlet boundaries.

interference from the second lamella in both, the Lomer and the collinear configuration.

Considering the extended formulation with the interaction matrix applied, a clear difference between the Lomer and the collinear configuration is visible due to the separation of interaction mechanisms as shown in fig. 7 (d,e). It can be seen, that even for a density equally distributed between slip systems, a higher coefficient accounting for the interaction between slip systems yields a significant reduction of density motion through the second lamella. Using the Taylor term, this is only observed if a heterogeneous density distribution is introduced on the slip systems (fig. 7c). Here, the interaction stress within the intersection is sufficiently lower than outside due to the higher density on the second slip system. In contrast, the corresponding results with the interaction matrix show nearly a complete stop of the dislocation motion at the core of the intersection area. It is also observed, that there is very little influence of the self-hardening coefficient in the vicinity of the intersection. This indicates, that the system is dominated by the strong collinear coefficient. Although the system of two slip lamellae is very artificial, it nevertheless can be concluded that the extended formulation allows for a more reasonable consideration of the different interaction mechanisms on different slip system in the considered setup.

To analyze the considered formulations in a configuration, which is not influenced by GND Pile-ups, we keep the configuration of two slip systems, but fill the whole cube with density and subject the system to a constant strain-rate. The respective stress-strain curves (fig. 8) show an elastic regime followed by a yield point, which is only slightly influenced by the considered strain rate. This observation is independent of the used interaction stress formulation and the subsequent plastic behavior is the same for different strain rates. However, the yield point can be significantly different depending on the considered coefficients (fig. 9). The findings are in accordance to the observations in the lamellae system - a lower influence of the self-hardening

is observed for the collinear configuration compared to the Lomer configuration. Although the same stress-strain curves can be achieved for both interaction stress formulations by choosing an adequate average coefficient in the Taylor term (fig. 9 a), the shortcoming of the Taylor coefficient can be observed if the density is increased on one of the slip systems as shown in fig. 9 (b) since self-hardening becomes the dominating effect. In contrast, the slip system with the higher density serves as a high resistance only to the primary slip system with lower density if the interaction matrix is applied. The interaction matrix leads to a complete deactivation of plastic slip on the slip system with lower density in the collinear case and thus an inhibition of the simultaneous activation of both collinear slip systems, i.e. collinear double slip, as observed in fig. 10 (a). In contrast, the Taylor term allows for collinear double slip since the same average coefficient α is applied to the primary as well as the secondary slip system.

Considering a system of equally distributed density but slightly different Schmid-factors for the two slip systems (due to a rotation of the crystal orientation by 4° around the [010] axis), it can be observed, that the collinear coefficient coupled with the lower self-hardening in the interaction matrix favors plastic slip on the dominating slip system, while the Taylor term yields a slip evolution according to the resolved shear stresses given by the Schmid-law (fig. 10 b). This indicates that considering both investigated formulations, only the interaction matrix is able to represent the inhibition of collinear double slip, which has been reported in the literature and has been introduced as an explanation for the pronounced instability of various tensile orientations with respect to small fluctuations in crystal orientation [35, 25, 24].

Expanding the analysis to all 12 fcc slip systems, we consider a system, which is again rotated by 4° around the [010] axis in order to get slightly different Schmid-factors on the slip systems. Using the interaction matrix, a concentration of the density can be observed on one of the collinear slip system pairings, which is already present at small strains. This is shown in fig. 11. In contrast, the results using the Taylor interaction stress still show Schmid-law behavior. Using a heterogeneous initial density distribution in the [001] high symmetry orientation, a similar concentration of the density on one of the collinear slip system pairings is observed. This indicates a general property of the interaction matrix to select one slip system of each collinear pairing in the analyzed heterogeneous configurations.

However, the impact of the differences of both formulations is dependent on the elastic stiffness of the system. This is illustrated by preventing the lateral displacement of the Dirichlet boundary conditions, which leads to a very similar density distribution for both formulations shown in fig. 12. In this case, the elastically stiffer behavior inhibits the relaxation of the system by single or double slip and leads to a density evolution according to the stresses given by the Schmid law. However, since the current analysis is restricted to small strains, it has to be further investigated whether this behavior holds also for larger strains, or whether the interaction matrix allows for a concentration of density on specific slip systems despite the stiffer boundary conditions.

Furthermore, it should be noted that due to the full interaction matrix with all coefficients assumed nonzero, the selection of one slip system of each collinear pairing might also depend on the values assumed for the weaker reaction types. However, the observed strong interaction between the two respective collinear systems (essentially preventing collinear double slip) is in agreement with published DDD-results [24, 25]. In addition, a high orientation dependency of the work hardening has been observed by experimental analyses for the [001] orientation [36]. This has been explained by the strong collinear interaction by [20, 19] which is in agreement with our observations. However, both formulations allow for collinear double slip in systems with homogeneous density distribution and resolved shear stresses as well as in systems in which a

relaxation on specific slip systems is inhibited due to boundary conditions. Therefore, the Taylor term is an adequate simplification of the interaction matrix in such high symmetry configurations, which can lead to a reduction of complexity in the continuum model.

The investigation shows promising results to reproduce DDD and experimental results from the literature. However, both formulations in the considered form only reduce the effective stress and always affect the total density of the respective slip systems. Dislocation transport between slip systems due to cross-slip and glissile reactions will have a significant effect on the resulting density distribution including a density deposition on zero Schmid-factor systems [37]. Both, cross-slip and glissile reactions are expected to affect the interaction between the respective glide systems or to feed into new glide systems. Both processes therefore need to be accounted for as mechanisms for dislocation density transport between slip systems in future continuum formulations. Furthermore, the shortcoming of both formulations applied here is the inability to represent the interaction mechanisms in the form of physical reactions or immobile structures and therefore contrasts with the idea of a largely immobile forest density. This suggests a discussion of the necessity to account for density immobilization and annihilation in dislocation based continuum models and the review of the assumption in the current formulation, that all dislocations are mobile.

5. Conclusion

In the present paper we analyze two commonly used flow stress formulations for a dislocation-density based continuum formulation of plasticity. Different combinations of possible interactions between slip systems are compared. As a central aspect, we address the question which level of homogenization is reasonable for the continuum modeling of dislocation interaction at intersections of slip systems. In this context, the impact of varying crystal orientation as well as homogeneously and inhomogeneously distributed dislocation density is analyzed.

The outcome of the present study is that averaging over all interaction types is a reasonable simplification for interaction stresses in high symmetry systems with reasonably homogeneous density distribution. For systems dominated by collinear interactions, an averaging of all interactions to one parameter is not sufficient. As soon as the stress or the density is inhomogeneous between slip systems, the collinear interaction enforces the density concentration on specific slip systems.

Thus, the key difference between the Taylor interaction stress and the interaction matrix is, that the Taylor term enables dislocation motion with respect to the Schmid stresses whereas the interaction matrix distinguishes dislocation mobility according to Schmid stress as well as density inhomogeneities between collinear systems. The latter yields a significantly different density evolution on slip systems with similar Schmid factors. This is in agreement with DDD findings in the literature.

However, this intrinsic impact of the collinear interaction is reduced again if boundary or interfacial conditions inhibit a relaxation on particular slip systems. This has been shown for an example system.

Acknowledgement

We would like to thank Daniel Weygand of KIT for the helpful discussion. This work was performed on the computational resource ForHLR II funded by the Ministry of Science, Research

and the Arts Baden-Wrttemberg and DFG ("Deutsche Forschungsgemeinschaft"). The Financial support for the research group FOR1650 *Dislocation based Plasticity* funded by the German Research Foundation (DFG) under the contract number GU367/36-2 as well as the support by the European Social Fund and the state of Baden-Wuerttemberg is gratefully acknowledged.

[1] N. Fleck, J. Hutchinson, Strain gradient plasticity, Advances in applied mechanics 33 (1997) 296–361.
[2] E. C. Aifantis, The physics of plastic deformation, International Journal of Plasticity 3 (3) (1987) 211–247.
[3] M. E. Gurtin, B. D. Reddy, Gradient single-crystal plasticity within a miseshill framework based on a new formulation of self- and latent-hardening, Journal of the Mechanics and Physics of Solids 68 (2014) 134 – 160.
[4] E. Bayerschen, M. Stricker, S. Wulfinghoff, D. Weygand, T. Böhlke, Equivalent plastic strain gradient plasticity with grain boundary hardening and comparison to discrete dislocation dynamics, in: Proc. R. Soc. A, Vol. 471, The Royal Society, 2015.
[5] S. Bargmann, B. D. Reddy, B. Klusemann, A computational study of a model of single-crystal strain-gradient viscoplasticity with an interactive hardening relation, International Journal of Solids and Structures 51 (15) (2014) 2754 – 2764.
[6] T. Hochrainer, S. Sandfeld, M. Zaiser, P. Gumbsch, Continuum dislocation dynamics: Towards a physical theory of crystal plasticity, Journal of the Mechanics and Physics of Solids 63 (2014) 167 – 178.
[7] T. Hochrainer, M. Zaiser, P. Gumbsch, A three-dimensional continuum theory of dislocation systems: kinematics and mean-field formulation, Philosophical Magazine 87 (8-9) (2007) 1261–1282.
[8] I. Groma, F. Csikor, M. Zaiser, Spatial correlations and higher-order gradient terms in a continuum description of dislocation dynamics, Acta Materialia 51 (5) (2003) 1271 – 1281.
[9] M. Zaiser, M.-C. Miguel, I. Groma, Statistical dynamics of dislocation systems: The influence of dislocation-dislocation correlations, Phys. Rev. B 64 (2001) 224102.
[10] G. I. Taylor, The mechanism of plastic deformation of crystals. part i. theoretical, Proceedings of the Royal Society of London. Series A, Containing Papers of a Mathematical and Physical Character 145 (855) (1934) 362–387.
[11] R. Madec, B. Devincre, L. Kubin, From dislocation junctions to forest hardening, Physical review letters 89 (25) (2002) 255508.
[12] P. Franciosi, M. Berveiller, A. Zaoui, Latent hardening in copper and aluminium single crystals, Acta Metallurgica 28 (3) (1980) 273–283.
[13] H. Mughrabi, The a-factor in the taylor flow-stress law in monotonic, cyclic and quasi-stationary deformations: Dependence on slip mode, dislocation arrangement and density, Current Opinion in Solid State and Materials Science 20 (6) (2016) 411–420.
[14] B. Devincre, L. Kubin, T. Hoc, Physical analyses of crystal plasticity by dd simulations, Scripta Materialia 54 (5) (2006) 741–746.
[15] R. Madec, L. P. Kubin, Dislocation strengthening in fcc metals and in bcc metals at high temperatures, Acta Materialia 126 (2017) 166–173.
[16] A. Alankar, I. N. Mastorakos, D. P. Field, H. M. Zbib, Determination of dislocation interaction strengths using discrete dislocation dynamics of curved dislocations, Journal of Engineering Materials and Technology 134 (2) (2012) 021018.
[17] D. Dickel, K. Schulz, S. Schmitt, P. Gumbsch, Dipole formation and yielding in a two-dimensional continuum dislocation model, Phys. Rev. B 90 (2014) 094118.
[18] C. Reuber, P. Eisenlohr, F. Roters, D. Raabe, Dislocation density distribution around an indent in single-crystalline nickel: Comparing nonlocal crystal plasticity finite-element predictions with experiments, Acta Materialia 71 (2014) 333 – 348.
[19] B. Devincre, T. Hoc, L. Kubin, Dislocation mean free paths and strain hardening of crystals, Science 320 (5884) (2008) 1745–1748.
[20] L. Kubin, B. Devincre, T. Hoc, Modeling dislocation storage rates and mean free paths in face-centered cubic crystals, Acta materialia 56 (20) (2008) 6040–6049.
[21] Y. Zhu, Y. Xiang, K. Schulz, The role of dislocation pile-up in flow stress determination and strain hardening, Scripta Materialia 116 (2016) 53 – 56.
[22] K. Schulz, M. Sudmanns, P. Gumbsch, Dislocation-density based description of the deformation of a composite material, Modelling and Simulation in Materials Science and Engineering 25 (6) (2017) 064003.
[23] K. Yoshida, A. Ishii, Y. Tadano, Work-hardening behavior of polycrystalline aluminum alloy under multiaxial stress paths, International Journal of Plasticity 53 (2014) 17–39.
[24] B. Devincre, L. Kubin, T. Hoc, Collinear superjogs and the low-stress response of fcc crystals, Scripta Materialia 57 (10) (2007) 905 – 908.
[25] B. Devincre, T. Hoc, L. P. Kubin, Collinear interactions of dislocations and slip systems, Materials Science and

Engineering: A 400401 (2005) 182 – 185.
[26] S. Schmitt, P. Gumbsch, K. Schulz, Internal stresses in a homogenized representation of dislocation microstructures, Journal of the Mechanics and Physics of Solids 84 (2015) 528–544.
[27] H. Mecking, U. F. Kocks, Kinetics of flow and strain-hardening, Acta Metallurgica 29 (11) (1981) 1865–1875.
[28] U. F. Kocks, H. Mecking, Physics and phenomenology of strain hardening: The fcc case, Progress in materials science 48 (3) (2003) 171–273.
[29] U. F. Kocks, A statistical theory of flow stress and work-hardening, Philosophical Magazine 13 (123) (1966) 541–566.
[30] M. Monavari, M. Zaiser, Annihilation and sources in continuum dislocation dynamics (CDD)arXiv:1709.03694.
[31] K. Schulz, L. Wagner, C. Wieners, A mesoscale approach for dislocation density motion using a runge-kutta discontinuous galerkin method, PAMM 16 (1) (2016) 403–404.
[32] C. Wieners, A geometric data structure for parallel finite elements and the application to multigrid methods with block smoothing, Computing and Visualization in Science 13 (4) 161–175.
[33] N. Hansen, X. Huang, Microstructure and flow stress of polycrystals and single crystals, Acta Materialia 46 (5) (1998) 1827 – 1836.
[34] S. Basinski, Z. Basinski, Plastic deformation and work hardening, Dislocations in solids 4 (1980) 261–362.
[35] L. Kubin, B. Devincre, T. Hoc, Toward a physical model for strain hardening in fcc crystals, Materials Science and Engineering: A 483 (2008) 19–24.
[36] T. Takeuchi, Orientation dependence of work hardening of copper single crystals near the [001] axis, Journal of the Physical Society of Japan 40 (3) (1976) 741–746.
[37] M. Stricker, D. Weygand, Dislocation multiplication mechanisms – glissile junctions and their role on the plastic deformation at the microscale, Acta Materialia 99 (2015) 130–139.